

Toward a universal description of hadronic phase of QCD

Aman Abhishek and Sayantan Sharma 

The Institute of Mathematical Sciences, a CI of Homi Bhabha National Institute, Chennai 600113, India



(Received 17 March 2023; accepted 15 December 2023; published 5 January 2024)

Mean-field model quantum field theories of hadrons were traditionally developed to describe cold and dense nuclear matter and are by now very well constrained from the recent neutron star merger observations. We show that when augmented with additional known hadrons and resonances but not included earlier, these mean-field models can be extended beyond its regime of applicability. Calculating some specific ratios of baryon number susceptibilities for finite temperature and moderate values of baryon densities within mean-field approximation, we show that these match consistently with the lattice QCD data available at lower densities, unlike the results obtained from a noninteracting hadron resonance gas model. We also estimate the curvature of the line of constant energy density, fixed at its corresponding value at the chiral crossover transition in QCD, in the temperature-density plane. The number density at low temperatures and high density is found to be about twice the nuclear saturation density. Moreover from this line we can indirectly constrain the critical endpoint of QCD to be beyond $\mu_B = 596$ MeV for temperature ~ 125 MeV.

DOI: [10.1103/PhysRevD.109.014007](https://doi.org/10.1103/PhysRevD.109.014007)

I. INTRODUCTION

Developing an effective field theory description of hadrons preceded the discovery of the field theory of strong interactions, quantum chromodynamics (QCD). Indeed, based on the observation of the exponential increase in the density of states of hadrons with increasing temperature, it was proposed that hadronic matter will undergo a phase transition to a deconfined phase [1]. *Ab initio* lattice studies have confirmed this scenario and showed the existence of a smooth crossover at zero baryon density [2–6] from a hadron phase to a quark-gluon plasma phase in $2 + 1$ flavor QCD with physical quark masses at a temperature $T_c = 156.5 \pm 1.5$ MeV [7]. Furthermore lattice QCD techniques have now provided us with the state-of-the-art equation of state (EoS) of hadrons in the continuum limit [8–10]. Such reliable results have boosted the efforts for understanding the different hadron interactions and develop effective relativistic quantum field theories of hadrons, the so-called *hadrodynamics*. Constraining *hadrodynamics* to a very good extent is of fundamental importance in understanding QCD at finite temperature and density.

A description of the hadron phase in terms of a gas of non-interacting hadrons and the narrow-width resonances

(HRG) [11–13] has been shown to describe bulk thermodynamic observables in QCD, e.g., free-energy [14–16] and chiral condensate [17,18] to a surprisingly good accuracy. This description is the basis for statistical hadronization models that have been very successful in describing the experimental yields of different hadron species in heavy-ion colliders [19]. A justification of this comparison came from the observation that nonresonant part of the phase shifts of the attractive hadron interactions largely cancel out in the calculation of free-energy, and the interacting part of the pressure can be well described by the contribution of resonances treated as stable particles [20]. However with increasing precision of the lattice data on fluctuations of conserved numbers like baryon number, strangeness and electric-charge, a visible departure from the HRG model predictions are by now clearly evident. Extension of the basic HRG model by augmenting it with the many not-yet experimentally measured baryon resonances [21] mainly in the strangeness sector [22], but predicted from lattice QCD and different relativistic quark models, termed as QMHRG can explain many puzzles like simultaneous freezeout of light, strange and open-charm hadrons [23–25]. However there are thermodynamic observables in QCD which cannot be yet explained within the QMHRG model, specially close to T_c [19,26,27], highlighting the importance of nonresonant and repulsive interaction channels. Moreover attempts have been made to extend HRG model to finite densities using van-der Waals inspired potentials [28,29] which has both attractive as well as repulsive interactions. However due to hard sphere interactions, the speed of sound exceeds that of the speed

Published by the American Physical Society under the terms of the Creative Commons Attribution 4.0 International license. Further distribution of this work must maintain attribution to the author(s) and the published article's title, journal citation, and DOI. Funded by SCOAP³.

of light at higher values of baryon densities which require further modifications [30]. In these extensions of the HRG model one cannot constraint the couplings from experimental data on nucleon-meson scatterings hence in order to understand hadrodynamics from a more fundamental perspective we need to choose a different approach.

Repulsive interactions between baryons will become more important at large baryon densities. However constraining them is challenging [31] as there are no first principles calculations of the EoS available yet from lattice QCD due to the infamous *sign-problem* [32,33]. Experimental constraints are also few and come mainly from the study of supernovae, neutron star mergers and nuclear matter from the intermediate energy heavy-ion collision experiments at CERN SPS and HADES, Darmstadt and in future from the upcoming FAIR facility at GSI Darmstadt and NICA at Dubna. Recent advances in the multi-messenger astronomy of neutron stars have opened a new avenue to constrain the nuclear models and its EoS [31,34,35]. In this regime of high baryon densities there are a multitude of nuclear models with different EoS. These are usually based on the Dirac-Brueckner-Hartree-Fock [36–38] approach or relativistic mean field models [39–41]. In the former approach parameters of the interactions are fixed from experimental inputs of nucleon-nucleon and nucleon-meson scatterings. However its application to finite density nuclear matter remains difficult. On the other hand in relativistic hadron models, pioneered by Walecka, the interactions between the nucleons are implemented at mean-field level by coupling to effective meson degrees of freedom. The parameters of the interaction terms are instead determined by matching to the empirical saturation properties of nuclear matter. Recent observation of a medium sized neutron star heavier than twice the solar mass [42–45], simultaneous mass radius measurements [46–50] and bounds on tidal deformability [51,52] during neutron star mergers have lead to more stringent constraints on the nuclear EoS [53–64] and hence on these mean-field models.

In this paper we address the question of how well these nuclear models which are traditionally designed to explain cold-dense nuclear matter, can describe QCD thermodynamics at a relatively higher temperatures and moderate baryon densities. By extending the study of relativistic hadron models (which are well constrained from neutron-star merger observations) to moderate values of baryon densities and higher temperatures, i.e., in the region $\mu_B/T = 3-5$, we estimate the hadronic freezeout line. Using the information about the pseudo-critical line at small baryon densities from lattice QCD, we constrain the location of the critical endpoint (CEP) at $\mu_{\text{CEP}}/T_{\text{CEP}} > 5$ if $T_{\text{CEP}} \sim 0.8 T_c$ [65]. The broad outline of the paper is as follows: we begin in the next section by introducing the specific relativistic mean-field hadron model used in this work. In the subsequent sections we calculate different thermodynamic observables within these mean-field models and compare to the lattice QCD results on thermodynamic susceptibilities at finite temperatures and moderate values of net-baryon densities. We show that these mean-field models can be very well extended beyond its traditional regime of application and in some cases can explain lattice data better than QMHRG. This has deeper implications and suggest that nonresonant interactions between the hadrons are crucial to explain the lattice QCD data at moderate baryon densities revealing the universal nature of hadronic interactions.

II. RELATIVISTIC MEAN-FIELD MODELS FOR HADRODYNAMICS

In order to choose a suitable starting point we consider a relativistic mean-field effective model which includes strange baryons [66]. This specific model along with other two models [67,68] are very well constrained out of many hadronic models using the latest gravitational wave data coming from neutron star mergers and experimental data on nuclear skin thickness [57]. Indeed the recent *ab initio* result for the neutron skin of Pb^{208} [69] is consistent with this model.

The Lagrangian of this effective model [66] is given as,

$$\begin{aligned} \mathcal{L} = & \sum_B \bar{\psi}_B [\gamma_\mu (i\partial^\mu - g_{\omega B}\omega^\mu - g_{\rho B}\rho^\mu \cdot \tau - g_{\phi B}\phi^\mu) - (M - g_{\sigma B}\sigma - g_{\delta B}\delta \cdot \tau - g_{\sigma_s B}\sigma_s)] \psi_B + \frac{1}{2} (\partial_\mu \sigma \partial^\mu \sigma - m_\sigma^2 \sigma^2) \\ & - \frac{1}{3} b_\sigma M (g_\sigma \sigma)^3 - \frac{1}{4} c_\sigma (g_\sigma \sigma)^4 - \frac{1}{4} (\omega_{\mu\nu} \omega^{\mu\nu}) + \frac{1}{2} m_\omega^2 (\omega_\mu \omega^\mu) + \frac{1}{4} c_\omega (g_\omega^2 \omega_\mu \omega^\mu)^2 + \frac{1}{2} (\partial_\mu \delta \partial^\mu \delta - m_\delta^2 \delta^2) \\ & + \frac{1}{2} m_\rho^2 \rho^\mu \cdot \rho_\mu - \frac{1}{4} (\rho_{\mu\nu} \cdot \rho^{\mu\nu}) + \frac{1}{2} \Lambda_V (g_\rho^2 \rho_\mu \cdot \rho^\mu) (g_\omega^2 \omega_\mu \omega^\mu) + \frac{1}{2} (\partial_\mu \sigma_s \partial^\mu \sigma_s - m_{\sigma_s}^2 \sigma_s^2) + \frac{1}{2} m_\phi^2 \phi_\mu \phi^\mu - \frac{1}{4} \phi_{\mu\nu} \phi^{\mu\nu}. \end{aligned}$$

We henceforth refer to this as model 1. In this model, the baryon fields ψ_B are coupled to the Lorentz scalar isoscalar σ, σ_s , vector isoscalar ω_μ, ϕ_μ , scalar isovector δ_i and vector isovector $\rho_{i\mu}$ meson fields respectively and τ is the isospin

matrix. The field strength tensor corresponding to vector meson ρ_μ is denoted as $\rho_{\mu\nu} = \partial_\mu \rho_\nu - \partial_\nu \rho_\mu - [\rho_\mu, \rho_\nu]$ and similarly defined for ϕ_μ fields as $\phi_{\mu\nu} = \partial_\mu \phi_\nu - \partial_\nu \phi_\mu$. The terms g_{aB} denotes the coupling of meson labeled by index a

to a baryon labeled by an index B . The couplings g_a without a second subscript B simply denotes the coupling of meson a to a nucleon. Interactions involving σ and ω mesons to nucleons are characterized by couplings g_σ, g_ω . These couplings along with terms b_σ and c_σ are important in obtaining the correct values for binding energy, saturation density and compressibility of infinite nuclear matter. The interactions mediated by δ and ρ -mesons involving couplings g_δ and Λ_V contribute to the asymmetry energy between protons and neutrons and is important for the stability of the nuclei drip line. One additionally has the hyperon interactions built in the same model. The strength of hyperon interactions are constrained from different sources. The coupling of hyperons to vector and isovector mesons, given by g_{ij} where i labels $\omega, \rho, \delta, \phi$ mesons and j labels Λ^0, Σ^- baryons, are constrained from $SU(6)$ symmetry within the quark model. Furthermore their couplings to scalar mesons σ and σ_s , denoted by $g_{\sigma j}$ and $g_{\sigma_s j}$ are constrained from the hyper-nuclear potentials in saturated nuclear matter. The strange mesons σ_s and ϕ play important role in accounting for hyperon-hyperon interactions [66]. We next calculate the Euler-Lagrange equations of motion for the meson fields. In the mean field approximation one neglects the spacetime dependence of the fields. Hence the space and time derivatives of fields are zero. For vector mean-fields, additionally, the time component is taken to have a nonzero mean-field value in order to maintain rotational symmetry. In case of scalar isovector δ field only its third component is assumed to have nonzero value and we represent it as δ_3 . The mean field equations which we solve comes out to be,

$$\begin{aligned}
m_\sigma^2 \sigma &= g_\sigma \left[\sum_B \frac{g_{\sigma B}}{g_\sigma} \rho_B^S - b_\sigma M (g_\sigma \sigma)^2 - c_\sigma (g_\sigma \sigma)^3 \right] \\
m_\omega^2 \omega_0 &= g_\omega \left[\sum_B \frac{g_{\omega B}}{g_\omega} \rho_B^B - c_\omega M (\omega_\mu \omega^\mu \omega_0) - g_\rho^2 \rho_\mu \cdot \rho^\mu \Lambda_V g_\omega \omega_0 \right] \\
m_\rho^2 \rho_{03} &= g_\rho \left[\sum_B \frac{g_{\rho B}}{g_\rho} \rho_B^B \tau_{3B} - g_\rho \rho_{03} \Lambda_V g_\omega^2 \omega_\mu \omega^\mu \right] \\
m_\delta^2 \delta_3 &= g_\delta \sum_B \frac{g_{\delta B}}{g_\delta} \rho_B^S \tau_{3B} \\
m_{\sigma_s}^2 \sigma_s &= g_{\sigma_s \Lambda} \sum_B \frac{g_{\sigma_s B}}{g_{\sigma_s \Lambda}} \rho_B^S \\
m_\phi^2 \phi_0 &= g_{\phi \Lambda} \sum_B \frac{g_{\phi B}}{g_{\phi \Lambda}} \rho_B^B.
\end{aligned} \tag{1}$$

The τ_{3B} represents isospin quantum number for baryon B and takes the values $\tau_{3B} = 1, -1, -1, 0$ for proton, neutron, Σ^- and Λ^0 respectively. In the mean field approximation, the vector meson fields V^μ satisfy, $V_\mu V^\mu = V^0{}^2$. For simplicity we will drop the subscripts and superscripts and refer to mean field values of vector fields simply as V .

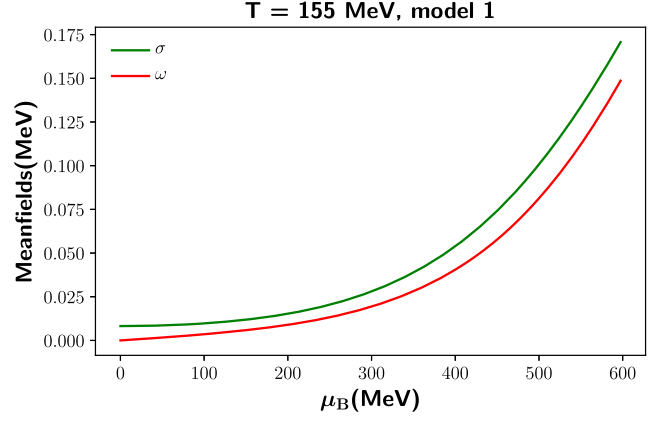


FIG. 1. σ and ω fields mean field values vs μ_B for $T = 155$ MeV. Other mean-fields are much smaller in magnitude compared to these data.

Once the values of mean-fields are known from the solutions of these equations satisfying the above constraint equations, the pressure can be calculated. The baryon and scalar densities ρ_B^B and ρ_B^S are defined in terms of the spin-degeneracy factors d_B corresponding to baryons and the Fermi-Dirac distributions $n(p), \bar{n}(p)$ for baryons and its anti-particles as,

$$\begin{aligned}
\rho_B^B &= d_B \int \frac{d^3 p}{(2\pi)^3} [n(p) - \bar{n}(p)], \\
\rho_B^S &= d_B \int \frac{d^3 p}{(2\pi)^3} \frac{M_B^*}{E_B^*(p)} [n(p) + \bar{n}(p)].
\end{aligned} \tag{2}$$

Here the medium modified masses and energies of baryons are defined as $M_B^* = M_B - g_{\sigma B} \sigma - g_{\delta B} \delta_3 \tau_3 - g_{\sigma_s B} \sigma_s$ and $E_B^*(p) = \sqrt{p^2 + M_B^{*2}}$. In Fig. 1 we have shown the mean-field values of σ, ω mesons in model 1 [66] as a function of the baryon chemical potential. From the plot we observe that as μ_B increases, the mean-field values of σ and ω fields also increases, hence the interactions mediated by these mesons become more relevant. This is because the mean-field values for σ and ω fields are proportional to scalar and baryon densities respectively, which increase with the baryon chemical potential. The ρ and δ mean-fields are proportional to the isospin baryon and scalar densities respectively. Since the isospin chemical potential is negligibly small, these mean-fields remain insignificant. The σ_s and ϕ_s mesons couple only to strange baryons which are heavy and thus their mean-field values remain small. The mean-fields which enhance the pressure correspond to mesons which mediate repulsive interactions and those which decreases the value of pressure correspond to those mediating attractive interactions. The ω thus mediates repulsive interactions and the σ , attractive interactions. It is also evident that the mean-values of the σ field are most sensitive to μ_B followed by the ω field. Hence for

$\mu_B < 300$ MeV, the attractive interactions due to σ dominates over the repulsive vector interactions due to ω mesons. Since the strange mesons are comparatively more massive, their mean-fields have a negligibly small dependence on μ_B .

One may note that while mean values of the fields other than σ and ω are tiny and hence not shown in Fig. 1, they play an important role at high densities and low temperatures in fitting with the experimental data, even though their contributions are subdominant. Recalling that the contribution from the ω mean field is essentially proportional to the baryon density at the mean-field level whereas that from the σ mean-field depends on the sum of baryon and anti-baryon densities. Hence the effect of repulsive ω interactions in thermodynamic observables are visible only at finite net-baryon density, within this approximation.

In this work we augment this basic model 1, which is well constrained at temperatures close to zero and large baryon densities, in order to describe hydrodynamics for a wide range of temperatures and densities. We define a model 2 in which we make the following extensions,

- (1) We include more baryons and mesons which are listed in the QMHRG model but not yet observed in the experiments.
- (2) We have not included any repulsive interactions among these augmented list of mesons. The attractive resonant interactions in the meson sector are implemented by including all possible resonances in the model 2 upto 3 GeV.
- (3) Adding more baryons to model 1 requires the knowledge of the couplings of these additional degrees of freedom to meson fields. These couplings cannot be fixed from experiments as not enough data is currently available.
- (4) As a first attempt we consider the couplings of all these extra baryons with mesons to be identically same, differentiating only on the basis of their strangeness content. The couplings of nonstrange baryon degrees of freedom with mesons are taken to be a fraction of nucleon-meson couplings and those of the additional strange baryons to mesons to be a fraction of Λ hyperon-meson couplings.
- (5) We introduce parameters α, α^S which are defined as $g^{B-M} = \alpha g^{N-M}$ and $g^{SB-M} = \alpha^S g^{\Lambda-M}$. The parameter α denote the strength of couplings of the additional QMHRG nonstrange baryons denoted by B and mesons compared to the nucleon N and meson M couplings present in model 1. Similarly α^S denotes a similar quantity for the baryons carrying strangeness quantum number denoted by the abbreviation SB .

We will first constrain the parameter space of α and α^S by comparing the results of different correlation data between baryon number, charge and strangeness quantum numbers calculated from the hadronic model 2 and those obtained

from lattice QCD. We will henceforth show our results at finite μ_B for two cases,

- (1) $n_Q/n_B = 0.4, \quad n_S = 0,$
- (2) $\mu_Q = 0, \quad \mu_S = 0.$

The condition (1), the so-called strangeness neutral conditions that are realized in a typical heavy-ion collision for the phase diagram. The constraint (2) corresponds to the case where most of the lattice QCD thermodynamics data are available for comparison. In these models the mean field values of meson fields at different temperature and densities are obtained by solving a set of self-consistent equations corresponding to different nucleon masses and energies, the details of which are discussed in the next section.

III. THERMODYNAMIC OBSERVABLES AND THEIR NUMERICAL IMPLEMENTATION

Given the Lagrangian of model 1, one can calculate [70] the pressure P , which at the mean-field level is,

$$\begin{aligned}
 P = & \sum_{i \in B} \frac{2}{3} \int \frac{d^3 p}{(2\pi)^3} \frac{p^2}{E_i^*(p)} [n_i(p) + \bar{n}_i(p)] - \frac{1}{2} m_\sigma^2 \sigma^2 \\
 & - \frac{1}{3} b_\sigma M (g_\sigma \sigma)^3 - \frac{1}{4} c_\sigma (g_\sigma \sigma)^4 + \frac{1}{2} m_\omega^2 \omega_0^2 \\
 & + \frac{1}{4} c_\omega (g_\omega^2 \omega_0^2)^2 - \frac{1}{2} m_\delta^2 \delta_3^2 + \frac{1}{2} m_\rho^2 \rho_{03}^2 \\
 & + \frac{1}{2} \Lambda_V (g_\rho^2 \rho_{03}^2) (g_\omega^2 \omega_0^2) - \frac{1}{2} m_{\sigma_s}^2 \sigma_s^2 + \frac{1}{2} m_\phi^2 \phi_0^2. \quad (3)
 \end{aligned}$$

Here $M_i^* = M_i - g_{\sigma i} \sigma - g_{\delta i} \delta_3 - g_{\rho i} \rho_{03} - g_{\phi i} \phi_0$ is the effective mass for i^{th} baryon where $i = p, n, \Lambda_0, \Sigma^-$ and $E_i^*(p) = \sqrt{p^2 + M_i^{*2}}$. The effective chemical potential is defined as $\mu_i^* = \mu_i - g_{\omega i} \omega_0 - g_{\rho i} \rho_{03} - g_{\phi i} \phi_0$. Using the relation $\epsilon = -P + Ts + \mu n_B$, we get the energy density,

$$\begin{aligned}
 \epsilon = & \sum_{i \in B} \int \frac{d^3 p}{(2\pi)^3} 2E_i^*(p) [n_i(p) + \bar{n}_i(p)] + \frac{1}{2} m_\sigma^2 \sigma^2 \\
 & + \frac{1}{3} b_\sigma M (g_\sigma \sigma)^3 + \frac{1}{4} c_\sigma (g_\sigma \sigma)^4 + \frac{1}{2} m_\omega^2 \omega_0^2 \\
 & + \frac{1}{4} c_\omega (g_\omega^2 \omega_0^2)^2 + \frac{1}{2} m_\delta^2 \delta_3^2 + \frac{1}{2} m_\rho^2 \rho_{03}^2 \\
 & + \frac{1}{2} \Lambda_V (g_\rho^2 \rho_{03}^2) (g_\omega^2 \omega_0^2) + \frac{1}{2} m_{\sigma_s}^2 \sigma_s^2 + \frac{1}{2} m_\phi^2 \phi_0^2, \quad (4)
 \end{aligned}$$

The susceptibilities corresponding to different conserved quantum number, i.e., baryon number (B), charge (Q), and strangeness (S) can be calculated from the partition function as,

$$\chi_{ijk}^{\text{BQS}} = -\frac{T}{V} \frac{\partial^{i+j+k} \ln \mathcal{Z}}{\partial \mu_B^i \mu_Q^j \mu_S^k}, \quad (5)$$

where i, j, k denote the order of derivative with respect to the chemical potentials μ_B, μ_Q, μ_S respectively. In what follows we are only interested in derivatives of pressure with respect to chemical potential and keep T constant while calculating derivatives. We schematically outline our numerical procedure for calculating the pressure and the different susceptibilities. We solve the following equations where X_i denote the meson mean-fields, μ_j the chemical potentials and \vec{f} denote the mean field Eqs. (1) in a compact form. The quantities \vec{g} denote the constraints (1), (2) on charge densities or chemical potentials,

$$\begin{aligned} \vec{f}(X_i, \mu_j, T) &= 0 \\ \vec{g}(X_i, \mu_j, T) &= 0. \end{aligned} \quad (6)$$

In order to calculate the derivative of pressure with respect to chemical potential μ_k , we need the derivatives of mean fields X and other chemical potentials $\mu_j, j \neq k$, with respect to μ_k . This is because X and $\mu_j, j \neq k$ depend on μ_k through gap and constraint equations respectively. Most often the first derivatives with respect to the chemical potential μ_k are calculated using the finite difference method with a grid $\delta\mu_k$ which is numerically accurate up to $\mathcal{O}(\delta\mu_k)$. Moreover the truncation error increases with increasing order of the derivatives. We thus follow a different procedure. Instead of performing a numerical differentiation, we use the gap and constraint equations to calculate the derivatives analytically. This is possible because the Eqs. (6) are satisfied at each value of T and μ_k in the parameter space of interest in this study hence these functions \vec{f}, \vec{g} are continuous and differentiable. The total derivative of each of Eq. (6) with respect to any chemical potential is zero in the mean-field approximation. Finding the derivatives of mean fields with respect to μ_k amounts to solving the following set of equations,

$$\begin{aligned} \frac{\partial \vec{f}}{\partial \mu_k} + \frac{\partial \vec{f}}{\partial X_i} \frac{dX_i}{d\mu_k} + \frac{\partial \vec{f}}{\partial \mu_j} \frac{d\mu_j}{d\mu_k} &= 0, \quad j \neq k, \\ \frac{\partial \vec{g}}{\partial \mu_k} + \frac{\partial \vec{g}}{\partial X_i} \frac{dX_i}{d\mu_k} + \frac{\partial \vec{g}}{\partial \mu_j} \frac{d\mu_j}{d\mu_k} &= 0. \end{aligned} \quad (7)$$

Due to the constraints $\vec{g}(X_i, \mu_j, T) = 0$, other chemical potentials μ_j are function of μ_k . Hence Eqs. (7) are two linear differential equations from which one can solve for the two unknowns $\frac{dX_i}{d\mu_k}$ and $\frac{d\mu_j}{d\mu_k}$. Obtaining these first order derivatives allows us to calculate the subsequent derivatives $\frac{d^n X_i}{d\mu_k^n}$ and $\frac{d^n \mu_j}{d\mu_k^n}, n \geq 2$ iteratively. Once the n^{th} order

derivatives of the mean-fields are known, the n^{th} order derivatives of pressure and hence the susceptibilities can be calculated.

IV. HOW CAN MEAN-FIELD MODELS BE EXTENDED TO EXPLAIN QCD THERMODYNAMICS IN T - μ_B PLANE

As mentioned earlier, the mean-field models were traditionally introduced to explain the nuclear liquid-gas transition in the $T \sim 0$ and large μ_B regime. We suggest here how we can extend the applicability of such models in the finite temperature and moderately high baryon number densities. We first study the ratio $\chi_{31}^{\text{BS}}/\chi_{11}^{\text{BS}}$ which motivates for the need to consider model 2 as the hadronic model which can describe QCD thermodynamics over a large range of T - μ_B values. This particular ratio $\chi_{31}^{\text{BS}}/\chi_{11}^{\text{BS}}$ in the extended model 2 is more sensitive to coupling α^S between strange baryons and mesons.

Since at the mean-field level we cannot include the effects of baryon-mediated repulsive interactions at $\mu_B = 0$ MeV, we cannot compare our results with lattice QCD results at zero baryon density. We thus show the data for this particular ratio as a function of μ_B at $T = 135$ MeV and $\mu_Q = \mu_S = 0$ in Fig. 2 for $\mu_B > 400$ MeV. As we extrapolate lattice results to finite density, their resultant error band increases. We thus choose a value of $\mu_B = 400$ MeV in order to have a sizeable effect of repulsive interactions on this observable in model 1 and 2 as well as a reasonably small error band on the lattice data. The upper limit of μ_B is chosen such that the energy density at $T = 135$ MeV is close to $\epsilon = 348 \pm 41$ MeV/fm³ which is the typical energy density at the chiral crossover transition [65]. The green band represents the results from lattice QCD [71] which is extrapolated up to $\mu_B = 400$ MeV. Results from QMHRG model and model 1 are also shown in the same plot from $\mu_B = 400$ MeV to

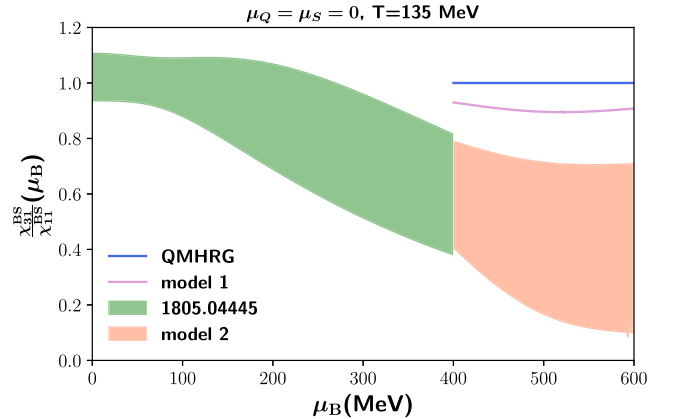


FIG. 2. The ratio $\chi_{31}^{\text{BS}}/\chi_{11}^{\text{BS}}$ from lattice QCD shown as green band compared to the corresponding results from ideal HRG shown in blue, model 1 in magenta and model 2 as an orange band.

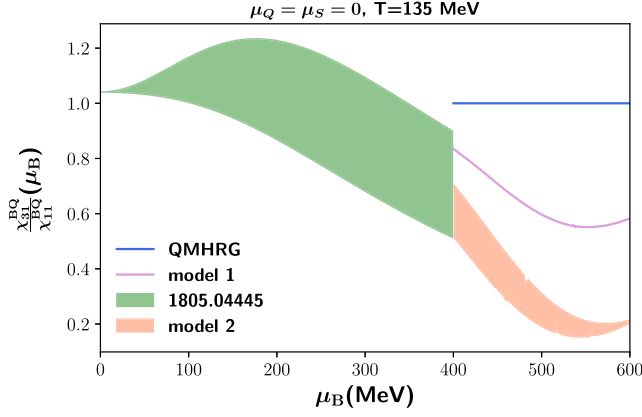


FIG. 3. The ratio $\chi_{31}^{\text{BQ}}/\chi_{11}^{\text{BQ}}$ from lattice QCD shown as green band compared to the corresponding results from ideal HRG shown in blue, model 1 in magenta and model 2 as an orange band.

$\mu_B = 600$ MeV as solid lines in the right hand corner. The results from model 1 are different from QMHRG model results and $\sim 12\%$ higher than the upper band of the lattice QCD result at $\mu_B = 400$ MeV. Thus while the inclusion of baryon-interactions inbuilt in model 1 improves the approach toward explaining the lattice data, clearly inclusion of just two strange baryons is not enough.

This discrepancy justifies the need for extending the model 1 to a model 2 which we have defined in the previous section. In order to constrain the parameters α and α^S , their values are varied such that the result of model 2 matches with the upper boundary of lattice QCD which gives a value of $\alpha = \alpha^S = 0.15$. If we also want to match the lower boundary of the lattice QCD result we have to choose the fractions as $\alpha = 0.2$ and $\alpha^S = 0.7$. Thus between the upper and lower edges of the lattice QCD band in Fig. 2, the nonstrange couplings change little while the strange couplings vary significantly. If the precision of the lattice QCD results could be improved it would allow us to quantify how strongly interacting the baryons are.

Now having fixed the couplings, we plot what are its implications for other thermodynamic observables. In Fig. 3 we study $\chi_{31}^{\text{BQ}}/\chi_{11}^{\text{BQ}}$ within the model 2. Comparing with the lattice QCD results we find that the results from model 1 already agrees with the lattice band but toward the upper edge of the band. Now calculating the same observable in the model 2 with additional hadrons, we find a much constrained region of match with the lattice QCD results shown as a green band, with the lower boundaries of these bands agreeing well at $\mu_B = 400$ MeV. Recall that the band in model 2 result comes from variation of α from 0.15 to 0.2 and α^S from 0.15 to 0.7.

We next show the results of another interesting observable χ_4^B/χ_2^B as a function of μ_B at $T = 135$ MeV and $\mu_Q = \mu_S = 0$ in Fig. 4. Again, the calculations within the model 1 agrees with the upper boundary of lattice QCD data band.

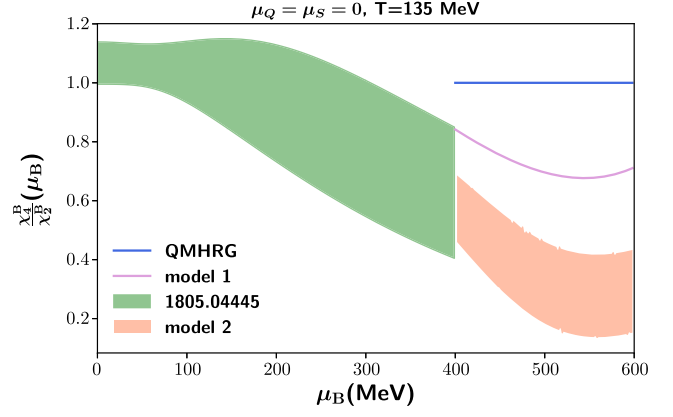


FIG. 4. The ratio χ_4^B/χ_2^B from lattice QCD shown as green band compared to the corresponding results from ideal HRG shown in blue, model 1 in magenta and model 2 as an orange band.

Using model 2, we find that the results of this ratio have a smaller spread due to the uncertainty in the values of the heavier baryon-meson couplings, compared to the current error band in the lattice QCD data. In fact the ratios χ_4^B/χ_2^B and $\chi_{31}^{\text{BQ}}/\chi_{11}^{\text{BQ}}$ is found to be more sensitive to nonstrange coupling α compared to α^S . We note that tuning the couplings (α, α_S) such that $\chi_{31}^{\text{BS}}/\chi_{31}^{\text{BS}}$ varies along the entire width of lattice band at $\mu_B = 400$ MeV, we get a variation of about only 50% in the quantities χ_4^B/χ_2^B and $\chi_{31}^{\text{BQ}}/\chi_{11}^{\text{BQ}}$. Thus the later two ratios can quite independently constrain the couplings than $\chi_{31}^{\text{BS}}/\chi_{31}^{\text{BS}}$. Thus to summarize the main findings of this section, we note that

- (1) A fit of with the coupling ratios (0.7, 0.2) for (α, α_S) was found to have a good match with all the three independent data on ratios of fluctuations obtained from lattice QCD.
- (2) For $\alpha = 0$, no value of α_S in the interval (0, 1) was found to completely cover the lattice error band in $\chi_{31}^{\text{BS}}/\chi_{11}^{\text{BS}}$, thus constraining the value of to have a lower bound $\alpha = 0.15$.
- (3) Typically larger values of α were found to violate lower bounds on χ_4^B/χ_2^B and $\chi_{31}^{\text{BQ}}/\chi_{11}^{\text{BQ}}$ obtained from the lattice QCD data hence can be now safely ignored with our analysis.

V. DO EXTENDED MEAN-FIELD MODELS SATISFY HIGH DENSITY CONSTRAINTS?

Since the model 1 satisfies very well the constraints from high density matter, like nuclear liquid-gas transition, neutron star EoS, etc, we would like to check whether augmenting this model with these additional hadrons would in anyway worsens this agreement. While the contribution of heavier baryons at high densities and low temperatures are expected to be suppressed due to the thermodynamic distribution functions, their multiplicities are large which could influence the thermodynamics despite suppression of

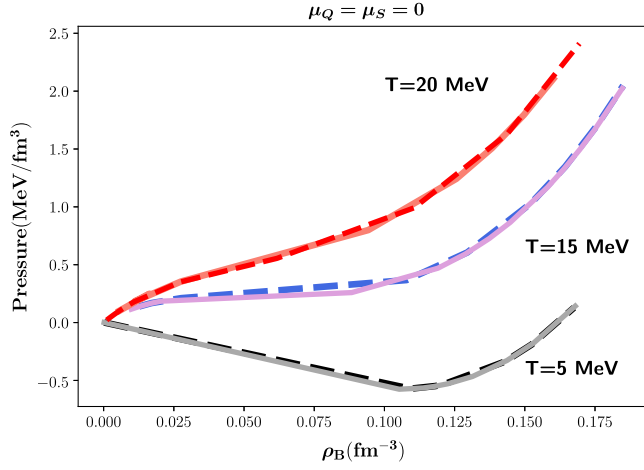


FIG. 5. Pressure versus baryon density curves for nuclear liquid gas transition. Dashed lines denote data from model 1 and solid lines are for model 2.

thermal distributions. To check how much of an impact these additional baryons will produce, we calculate the pressure as a function of baryon densities within model 1 and model 2 for three different temperatures $T = 5, 15, 20$ MeV respectively. The couplings used for model 2 are $\alpha = 0.2$ and $\alpha^S = 0.7$. The results of our calculation are shown in Fig. 5 as solid lines for model 2 which is compared with the dashed lines in the same plot which were estimated within the model 1. As clearly seen from the plot, extending the model with the additional baryons from QMHRG model even with larger allowed values of coupling doesn't affect the pressure plots significantly. This gives us a proof of principle that extending mean-field nuclear models with additional baryons to explain QCD thermodynamics at high temperatures and intermediate densities will not affect its already excellent agreement at high densities and low temperatures. Our approach indeed hints to a method toward formulating a universal theory describing the hadronic phase of QCD.

VI. IMPLICATIONS FOR THE PHASE DIAGRAM OF QCD

Having discussed the susceptibilities in the mean-field nuclear model and its extended version, we study what insights it could give us about the phase diagram of QCD. Nuclear mean-field models do not have the $U_L(2) \times U_R(2)$ chiral symmetries in-built like the Nambu-Jona-Lasinio model and hence cannot describe its restoration. We thus determine the line of constant energy density in the $T - \mu_B$ plane for these models by setting $\epsilon = 348 \pm 41$ MeV/fm³ [65] which is the energy density of 2 + 1 flavor QCD at the crossover region for $\mu_B = 0$ MeV. Unlike in traditional QMHRG model, recent lattice studies have observed that the energy density along the chiral crossover line does not vary with increasing μ_B at least

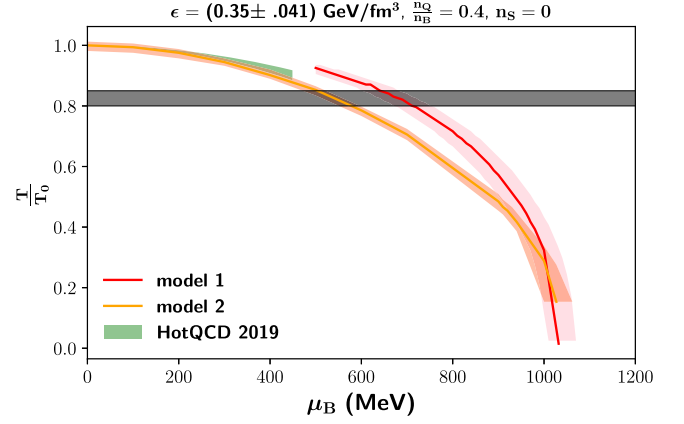


FIG. 6. Lines of constant energy density for model 1 shown in pink band and model 2 shown in orange band. Also shown is the crossover transition from lattice QCD in green band.

around $\mu_B/T \lesssim 3$ [72]. Incidentally the line of chemical freezeout of hadrons is also defined at a constant energy density [73,74] and it approaches the chiral crossover transition line as one goes to smaller values of μ_B . The results of our calculations of lines of constant energy density model 1 and 2 are shown in Fig. 6. These can be visualized as a chemical freezeout line for the hadrons present within the model. Indeed the line of constant energy density in model 2 is consistent with the latest continuum extrapolated lattice QCD data, all the way from $\mu_B = 0$ MeV (extrapolated) to about $\mu_B = 450$ MeV. There is a small difference between these two results which can be accounted for from the fact that the repulsive interactions present among the hadrons are not included within model 2. Since the model 2 has more degrees of freedom, its line of constant energy density deviates from the model 1 calculation for $\mu_B < 900$ MeV. At higher values of μ_B , the contributions of the heavier baryons and mesons to the energy density gets suppressed due to their mass and due to lowering of temperature respectively, hence the lines of constant energy between model 2 and its extended version start to agree. Another prominent feature of the QCD phase diagram is the anticipated critical endpoint (CEP) of the line of first order transitions. From the constraint that the CEP will exist in the real- μ_B plane, and its location gives the radius of convergence of thermodynamic observables, all orders of baryon number fluctuations have to be positive. Using this constraint from the lattice QCD data of upto 8-th order baryon number fluctuations at $\mu_B = 0$ [65], it is now known that $T_{\text{CEP}}/T_c < 0.85$. Noting this constraint by choosing the ratio $T/T(\mu_B = 0) = 0.8$ within the model 2 we can conclude that the CEP, if present will be at $\mu_B > 596$ MeV which provides a lower bound $\mu_B/T \sim 4.76$.

Next we calculate the curvature of these constant energy lines by fitting to the ansatz $\frac{T(\mu_B)}{T_c} = 1 - \kappa_2 \frac{\mu_B^2}{T_c^2} - \kappa_4 \frac{\mu_B^4}{T_c^4} - \kappa_6 \frac{\mu_B^6}{T_c^6}$. For model 1, the extracted curvature

coefficients are $\kappa_2 = 0.020(2)$, $\kappa_4 = -0.0010(3)$, $\kappa_6 = 0.000060(3)$ which are also consistent with those calculated from model 2, $\kappa_2 = 0.020(2)$, $\kappa_4 = -0.0005(1)$, and $\kappa_6 = 0.000010(2)$. The values of κ_2 are somewhat larger than the latest continuum extrapolated lattice results of the κ_2 [65,75,76] extracted from the renormalized chiral condensate and from a recent HRG model estimate [18], which is expected as the results from these models are for the entire $T-\mu_B$ plane. The value of κ_4 from lattice QCD is consistent with zero [65,76], whereas we find a negative but finite value in both the models. The results for κ_6 are new and it is about 1000 times smaller than κ_2 . Thus its effect should start become significant at $\mu_B/T \sim 15$, well within the cold nuclear matter regime. Moreover the baryon densities obtained in model 1 and 2 for a typical neutron star environment characterized with $n_Q/n_B = 0.05 - 0.2$, $n_S = 0$, varies from 0.28 fm^{-3} to 0.35 fm^{-3} as energy density varies from $\epsilon = 307-389 \text{ MeV/fm}^3$. The variation in the ratio for n_Q/n_B has a tiny effect on this density. It is remarkable that the typical nuclear densities we obtain from these models are about twice the nuclear saturation density, when many-body interactions start to become dominant [77] and quark exchanges are expected to mediate baryon interactions [78]. Our calculations also support this picture albeit indirectly that a mixed phase of quarks and hadrons can survive in neutron star cores with baryon densities greater than 0.35 fm^{-3} .

VII. IMPLICATIONS OF LATTICE QCD DATA AT $\mu_B = 0$ FOR HIGH DENSITY MODELS

Comparisons of lattice QCD data with QMHRG model particularly for observables like χ_4^B/χ_2^B [26] and higher order baryon number susceptibilities [16] clearly highlight the importance of including repulsive interactions within the QMHRG model. In our present study of nuclear model quantum field theories, the repulsive interactions at low baryon densities are negligible at the mean-field level. Unless there is a mechanism by which sufficient strength of repulsive interactions are generated at low baryon densities by calculating beyond mean-field, it would then imply that these models require suitable modifications to account for such interactions. In this way one can achieve a universal hadronic model, which is valid for both lower as well as high baryon densities. Furthermore our comparison of quantities like $\chi_{31}^{BS}/\chi_{11}^{BS}$ with the lattice data to extract the baryon-meson couplings in the extended model 2, will benefit from an increasing precision of the lattice QCD data. This will allow for a tighter constraint on the values of the couplings of strange baryons with mesons.

VIII. CONCLUSIONS

We started this work with a question of how well the traditional nuclear mean-field models, developed for the

understanding of physics at low temperatures and large baryon densities be used to explain QCD thermodynamics at high temperatures and moderate densities. A remarkable observation that comes out of our study is that augmenting these simple models with a complete list of baryons present in QMHRG model and tuning the couplings of their interactions with mesons through a comparison with lattice QCD data on a particular observable, lead to a very good description of QCD thermodynamics at intermediate densities. In our investigation we have found that the simple baryon-meson interactions built within the nuclear models are important in bridging the gap between lattice and other noninteracting hadron models like QMHRG. Furthermore we have shown that the inclusion of these additional hadrons do not affect the nuclear liquid-gas transition, which is well-studied in the original versions of these mean-field models.

This allows for a route to identify the relevant baryon interactions in chiral symmetry broken phase, which indeed if accounted for correctly will be valid for the entire regime of densities and temperatures. However at present there are not much data available, either from experiments or theory in constraining most of these baryon-meson couplings. Our method for determining these couplings from comparison with a particular thermodynamic observable from lattice, is one such possibility since in this process the benchmark data comes from the fundamental theory of strong interactions, i.e., QCD. We highlighted the need of high-precision lattice data which will allow for constraining such couplings further. This will allow for a better synergy between lattice QCD and such model quantum field theory calculations in future.

There are several directions still remains to be explored. Firstly it would be interesting to extend this study beyond the mean-field approximation and check whether it can account for the repulsive interactions that exist among baryons and mesons, even at low densities and high temperatures, evident from comparisons of lattice QCD data with QMHRG model. Another aspect toward building a universal hadronic model requires high density nuclear models to incorporate spontaneous chiral symmetry breaking. This can be achieved by including parity doublet partners like the pion degrees of freedom and the critical σ -modes, important for understanding the nature of the chiral phase transition at high densities and the thermodynamics near the critical endpoint.

ACKNOWLEDGMENTS

S. S. gratefully acknowledges support from the Department of Science and Technology, Government of India through a Ramanujan Fellowship. We would like to thank Deeptak Biswas, Jishnu Goswami, Hiranmaya Mishra and Jan Pawlowski for helpful discussions and correspondence.

- [1] R. Hagedorn, Statistical thermodynamics of strong interactions at high-energies, *Nuovo Cimento Suppl.* **3**, 147 (1965).
- [2] Y. Aoki, G. Endrodi, Z. Fodor, S. D. Katz, and K. K. Szabo, The order of the quantum chromodynamics transition predicted by the standard model of particle physics, *Nature (London)* **443**, 675 (2006).
- [3] A. Bazavov *et al.*, The chiral and deconfinement aspects of the QCD transition, *Phys. Rev. D* **85**, 054503 (2012).
- [4] T. Bhattacharya *et al.*, QCD phase transition with chiral quarks and physical quark masses, *Phys. Rev. Lett.* **113**, 082001 (2014).
- [5] F. Burger, E.-M. Ilgenfritz, M. P. Lombardo, and A. Trunin, Chiral observables and topology in hot QCD with two families of quarks, *Phys. Rev. D* **98**, 094501 (2018).
- [6] Y. Taniguchi, S. Ejiri, K. Kanaya, M. Kitazawa, H. Suzuki, and T. Umeda, $N_f = 2 + 1$ QCD thermodynamics with gradient flow using two-loop matching coefficients, *Phys. Rev. D* **102**, 014510 (2020); **102**, 059903(E) (2020).
- [7] A. Bazavov *et al.*, Chiral crossover in QCD at zero and nonzero chemical potentials, *Phys. Lett. B* **795**, 15 (2019).
- [8] S. Borsanyi, Z. Fodor, C. Hoelbling, S. D. Katz, S. Krieg, and K. K. Szabo, Full result for the QCD equation of state with $2 + 1$ flavors, *Phys. Lett. B* **730**, 99 (2014).
- [9] A. Bazavov *et al.*, Equation of state in $(2 + 1)$ -flavor QCD, *Phys. Rev. D* **90**, 094503 (2014).
- [10] H. T. Ding, S. Mukherjee, H. Ohno, P. Petreczky, and H. P. Schadler, Diagonal and off-diagonal quark number susceptibilities at high temperatures, *Phys. Rev. D* **92**, 074043 (2015).
- [11] R. Dashen, S.-K. Ma, and H. J. Bernstein, S matrix formulation of statistical mechanics, *Phys. Rev.* **187**, 345 (1969).
- [12] R. F. Dashen and R. Rajaraman, Narrow resonances in statistical mechanics, *Phys. Rev. D* **10**, 694 (1974).
- [13] R. F. Dashen and R. Rajaraman, Effective elementarity of resonances and bound states in statistical mechanics, *Phys. Rev. D* **10**, 708 (1974).
- [14] F. Karsch, K. Redlich, and A. Tawfik, Hadron resonance mass spectrum and lattice QCD thermodynamics, *Eur. Phys. J. C* **29**, 549 (2003).
- [15] F. Karsch, K. Redlich, and A. Tawfik, Thermodynamics at nonzero baryon number density: A comparison of lattice and hadron resonance gas model calculations, *Phys. Lett. B* **571**, 67 (2003).
- [16] P. Huovinen and P. Petreczky, QCD equation of state and hadron resonance gas, *Nucl. Phys.* **A837**, 26 (2010).
- [17] S. Borsanyi, Z. Fodor, C. Hoelbling, S. D. Katz, S. Krieg, C. Ratti, and K. K. Szabo, Is there still any T_c mystery in lattice QCD? Results with physical masses in the continuum limit III, *J. High Energy Phys.* **09** (2010) 073.
- [18] D. Biswas, P. Petreczky, and S. Sharma, Chiral condensate from a hadron resonance gas model, *Phys. Rev. C* **106**, 045203 (2022).
- [19] A. Andronic, P. Braun-Munzinger, K. Redlich, and J. Stachel, Decoding the phase structure of QCD via particle production at high energy, *Nature (London)* **561**, 321 (2018).
- [20] R. Venugopalan and M. Prakash, Thermal properties of interacting hadrons, *Nucl. Phys.* **A546**, 718 (1992).
- [21] A. Majumder and B. Muller, Hadron mass spectrum from lattice QCD, *Phys. Rev. Lett.* **105**, 252002 (2010).
- [22] A. Bazavov *et al.*, Strangeness at high temperatures: From hadrons to quarks, *Phys. Rev. Lett.* **111**, 082301 (2013).
- [23] A. Bazavov *et al.*, Additional strange hadrons from QCD thermodynamics and strangeness freezeout in heavy ion collisions, *Phys. Rev. Lett.* **113**, 072001 (2014).
- [24] A. Bazavov *et al.*, The melting and abundance of open charm hadrons, *Phys. Lett. B* **737**, 210 (2014).
- [25] S. Mukherjee, P. Petreczky, and S. Sharma, Charm degrees of freedom in the quark gluon plasma, *Phys. Rev. D* **93**, 014502 (2016).
- [26] D. Bollweg, J. Goswami, O. Kaczmarek, F. Karsch, S. Mukherjee, P. Petreczky, C. Schmidt, and P. Scior, Second order cumulants of conserved charge fluctuations revisited: Vanishing chemical potentials, *Phys. Rev. D* **104**, 074512 (2021).
- [27] J. M. Karthein, V. Koch, C. Ratti, and V. Vovchenko, Constraining the hadronic spectrum and repulsive interactions in a hadron resonance gas via fluctuations of conserved charges, *Phys. Rev. D* **104**, 094009 (2021).
- [28] V. Vovchenko, M. I. Gorenstein, and H. Stoecker, van der Waals interactions in hadron resonance gas: From nuclear matter to lattice QCD, *Phys. Rev. Lett.* **118**, 182301 (2017).
- [29] V. Vovchenko, A. Motornenko, P. Alba, M. I. Gorenstein, L. M. Satarov, and H. Stoecker, Multicomponent van der Waals equation of state: Applications in nuclear and hadronic physics, *Phys. Rev. C* **96**, 045202 (2017).
- [30] Y. Fujimoto, K. Fukushima, Y. Hidaka, A. Hiraguchi, and K. Iida, Equation of state of neutron star matter and its warm extension with an interacting hadron resonance gas, *Phys. Lett. B* **835**, 137524 (2022).
- [31] A. Lovato *et al.*, Long range plan: Dense matter theory for heavy-ion collisions and neutron stars, [arXiv:2211.02224](https://arxiv.org/abs/2211.02224).
- [32] P. de Forcrand, Simulating QCD at finite density, *Proc. Sci. LAT2009* (2009) 010.
- [33] C. Schmidt and S. Sharma, The phase structure of QCD, *J. Phys. G* **44**, 104002 (2017).
- [34] E. Annala, T. Gorda, E. Katerini, A. Kurkela, J. Nättilä, V. Paschalidis, and A. Vuorinen, Multimessenger constraints for ultradense matter, *Phys. Rev. X* **12**, 011058 (2022).
- [35] K. Sumiyoshi, T. Kojo, and S. Furusawa, Equation of state in neutron stars and supernovae, in *Handbook of Nuclear Physics* (Springer, Singapore, 2023), [10.1007/978-981-15-8818-1_104-1](https://doi.org/10.1007/978-981-15-8818-1_104-1).
- [36] R. Brockmann and R. Machleidt, Nuclear saturation in a relativistic Bruckner-Hartree-Fock approach, *Phys. Lett.* **149B**, 283 (1984).
- [37] B. Ter Haar and R. Malfliet, Nucleons, mesons and deltas in nuclear matter. A relativistic Dirac-Bruckner approach, *Phys. Rep.* **149**, 207 (1987).
- [38] F. de Jong and H. Lenske, Asymmetric nuclear matter in the relativistic Bruckner Hartree-Fock approach, *Phys. Rev. C* **57**, 3099 (1998).
- [39] B. D. Serot and J. D. Walecka, The relativistic nuclear many body problem, *Adv. Nucl. Phys.* **16**, 1 (1986).
- [40] B. D. Serot and J. D. Walecka, Recent progress in quantum hydrodynamics, *Int. J. Mod. Phys. E* **6**, 515 (1997).
- [41] A. R. Bodmer, Relativistic mean field theory of nuclei with a vector meson self-interaction, *Nucl. Phys.* **A526**, 703 (1991).

- [42] B. Margalit and B. D. Metzger, Constraining the maximum mass of neutron stars from multi-messenger observations of GW170817, *Astrophys. J. Lett.* **850**, L19 (2017).
- [43] M. Shibata, S. Fujibayashi, K. Hotokezaka, K. Kiuchi, K. Kyutoku, Y. Sekiguchi, and M. Tanaka, Modeling GW170817 based on numerical relativity and its implications, *Phys. Rev. D* **96**, 123012 (2017).
- [44] L. Rezzolla, E. R. Most, and L. R. Weih, Using gravitational-wave observations and quasi-universal relations to constrain the maximum mass of neutron stars, *Astrophys. J. Lett.* **852**, L25 (2018).
- [45] M. Ruiz, S. L. Shapiro, and A. Tsokaros, GW170817, general relativistic magnetohydrodynamic simulations, and the neutron star maximum mass, *Phys. Rev. D* **97**, 021501 (2018).
- [46] T. E. Riley *et al.*, A NICER View of PSR J0030 + 0451: Millisecond pulsar parameter estimation, *Astrophys. J. Lett.* **887**, L21 (2019).
- [47] M. C. Miller *et al.*, PSR J0030 + 0451 mass and radius from NICER data and implications for the properties of neutron star matter, *Astrophys. J. Lett.* **887**, L24 (2019).
- [48] T. E. Riley *et al.*, A NICER view of the massive pulsar PSR J0740 + 6620 informed by radio timing and XMM-Newton spectroscopy, *Astrophys. J. Lett.* **918**, L27 (2021).
- [49] M. C. Miller *et al.*, The radius of PSR J0740 + 6620 from NICER and XMM-Newton data, *Astrophys. J. Lett.* **918**, L28 (2021).
- [50] E. Fonseca *et al.*, Refined mass and geometric measurements of the high-mass PSR J0740 + 6620, *Astrophys. J. Lett.* **915**, L12 (2021).
- [51] B. P. Abbott *et al.*, GW170817: Observation of gravitational waves from a binary neutron star inspiral, *Phys. Rev. Lett.* **119**, 161101 (2017).
- [52] T. Hinderer, B. D. Lackey, R. N. Lang, and J. S. Read, Tidal deformability of neutron stars with realistic equations of state and their gravitational wave signatures in binary inspiral, *Phys. Rev. D* **81**, 123016 (2010).
- [53] F. Douchin and P. Haensel, A unified equation of state of dense matter and neutron star structure, *Astron. Astrophys.* **380**, 151 (2001).
- [54] K. Chatziioannou, K. Yagi, A. Klein, N. Cornish, and N. Yunes, Probing the internal composition of neutron stars with gravitational waves, *Phys. Rev. D* **92**, 104008 (2015).
- [55] E. Annala, T. Gorda, A. Kurkela, and A. Vuorinen, Gravitational-wave constraints on the neutron-star-matter equation of state, *Phys. Rev. Lett.* **120**, 172703 (2018).
- [56] I. Tews, J. Margueron, and S. Reddy, Critical examination of constraints on the equation of state of dense matter obtained from GW170817, *Phys. Rev. C* **98**, 045804 (2018).
- [57] R. Nandi, P. Char, and S. Pal, Constraining the relativistic mean-field model equations of state with gravitational wave observations, *Phys. Rev. C* **99**, 052802 (2019).
- [58] L. McLerran and S. Reddy, Quarkyonic matter and neutron stars, *Phys. Rev. Lett.* **122**, 122701 (2019).
- [59] E. Annala, T. Gorda, A. Kurkela, J. Nättilä, and A. Vuorinen, Evidence for quark-matter cores in massive neutron stars, *Nat. Phys.* **16**, 907 (2020).
- [60] M. M. Forbes, S. Bose, S. Reddy, D. Zhou, A. Mukherjee, and S. De, Constraining the neutron-matter equation of state with gravitational waves, *Phys. Rev. D* **100**, 083010 (2019).
- [61] G. Baym, S. Furusawa, T. Hatsuda, T. Kojo, and H. Togashi, New neutron star equation of state with quark-hadron crossover, *Astrophys. J.* **885**, 42 (2019).
- [62] C. Drischler, S. Han, J. M. Lattimer, M. Prakash, S. Reddy, and T. Zhao, Limiting masses and radii of neutron stars and their implications, *Phys. Rev. C* **103**, 045808 (2021).
- [63] T. Kojo, D. Hou, J. Okafor, and H. Togashi, Phenomenological QCD equations of state for neutron star dynamics: Nuclear-2SC continuity and evolving effective couplings, *Phys. Rev. D* **104**, 063036 (2021).
- [64] C. Drischler, R. J. Furnstahl, J. A. Melendez, and D. R. Phillips, How well do we know the neutron-matter equation of state at the densities inside neutron stars? A Bayesian approach with correlated uncertainties, *Phys. Rev. Lett.* **125**, 202702 (2020).
- [65] A. Bazavov *et al.*, The QCD equation of state to $\mathcal{O}(\mu_B^6)$ from lattice QCD, *Phys. Rev. D* **95**, 054504 (2017).
- [66] J. K. Bunta and S. Gmuca, Hyperons in a relativistic mean-field approach to asymmetric nuclear matter, *Phys. Rev. C* **70**, 054309 (2004).
- [67] B. Liu, V. Greco, V. Baran, M. Colonna, and M. Di Toro, Asymmetric nuclear matter: The role of the isovector scalar channel, *Phys. Rev. C* **65**, 045201 (2002).
- [68] S. Typel and H. H. Wolter, Relativistic mean field calculations with density dependent meson nucleon coupling, *Nucl. Phys.* **A656**, 331 (1999).
- [69] B. Hu *et al.*, *Ab initio* predictions link the neutron skin of ^{208}Pb to nuclear forces, *Nat. Phys.* **18**, 1196 (2022).
- [70] A. Schmitt, *Dense Matter in Compact Stars: A Pedagogical Introduction* (Springer Berlin, Heidelberg, 2010), Vol. 811.
- [71] S. Borsanyi, Z. Fodor, J. N. Guenther, S. K. Katz, K. K. Szabo, A. Pasztor, I. Portillo, and C. Ratti, Higher order fluctuations and correlations of conserved charges from lattice QCD, *J. High Energy Phys.* **10** (2018) 205.
- [72] D. Bollweg, D. A. Clarke, J. Goswami, O. Kaczmarek, F. Karsch, S. Mukherjee, P. Petreczky, C. Schmidt, and S. Sharma, Equation of state and speed of sound of (2 + 1)-flavor QCD in strangeness-neutral matter at non-vanishing net baryon-number density, *Phys. Rev. D* **108**, 014510 (2023).
- [73] F. Becattini, M. Gazdzicki, and J. Sollfrank, On chemical equilibrium in nuclear collisions, *Eur. Phys. J. C* **5**, 143 (1998).
- [74] D. Teaney, Chemical freezeout in heavy ion collisions, 2002.
- [75] C. Bonati, M. D'Elia, F. Negro, F. Sanfilippo, and K. Zambello, Curvature of the pseudocritical line in QCD: Taylor expansion matches analytic continuation, *Phys. Rev. D* **98**, 054510 (2018).
- [76] S. Borsanyi, Z. Fodor, J. N. Guenther, R. Kara, S. D. Katz, P. Parotto, A. Pasztor, C. Ratti, and K. K. Szabo, QCD crossover at finite chemical potential from lattice simulations, *Phys. Rev. Lett.* **125**, 052001 (2020).
- [77] A. Akmal, V. R. Pandharipande, and D. G. Ravenhall, The equation of state of nucleon matter and neutron star structure, *Phys. Rev. C* **58**, 1804 (1998).
- [78] K. Fukushima, T. Kojo, and W. Weise, Hard-core deconfinement and soft-surface delocalization from nuclear to quark matter, *Phys. Rev. D* **102**, 096017 (2020).